

 Open access • Journal Article • DOI:10.1021/ACS.JPCA.7B06119

Theoretical and Shock Tube Study of the Rate Constants for Hydrogen Abstraction Reactions of Ethyl Formate. — [Source link](#)

[Junjun Wu](#), [Fethi Khaled](#), [Hongbo Ning](#), [Liu hao Ma](#) ...+2 more authors





Institutions: [King Abdullah University of Science and Technology](#)

Published on: 14 Aug 2017 - [Journal of Physical Chemistry A](#) (American Chemical Society)

Topics: [Hydrogen atom abstraction](#), [Chemical kinetics](#), [Reaction rate constant](#), [Transition state](#) and [Transition state theory](#)

Related papers:

- [Theoretical chemical kinetic study of the H-atom abstraction reactions from aldehydes and acids by \$\dot{\text{H}}\$ atoms and \$\dot{\text{O}}\text{H}\$, \$\text{H}\dot{\text{O}}2\$, and \$\dot{\text{C}}\text{H}3\$ radicals.](#)
- [Theoretical studies on gas-phase kinetics and mechanism of H-abstraction reaction from methanol by ClO and BrO radicals](#)
- [Theoretical study of the rate constants for the hydrogen atom abstraction reactions of esters with \$\(\bullet\)\text{OH}\$ radicals.](#)
- [High temperature rate constants for H/D + methyl formate and methyl acetate](#)
- [The Penetration of a Potential Barrier by Electrons](#)

Share this paper:    

View more about this paper here: <https://typeset.io/papers/theoretical-and-shock-tube-study-of-the-rate-constants-for-36f86h1ov5>

Theoretical and Shock Tube Study of the Rate Constants for Hydrogen Abstraction Reactions of Ethyl Formate

Junjun Wu, Fethi Khaled, Hongbo Ning, Liuha Ma, Aamir Farooq, and Wei Ren

J. Phys. Chem. A, **Just Accepted Manuscript** • DOI: 10.1021/acs.jpca.7b06119 • Publication Date (Web): 03 Aug 2017

Downloaded from <http://pubs.acs.org> on August 8, 2017

Just Accepted

“Just Accepted” manuscripts have been peer-reviewed and accepted for publication. They are posted online prior to technical editing, formatting for publication and author proofing. The American Chemical Society provides “Just Accepted” as a free service to the research community to expedite the dissemination of scientific material as soon as possible after acceptance. “Just Accepted” manuscripts appear in full in PDF format accompanied by an HTML abstract. “Just Accepted” manuscripts have been fully peer reviewed, but should not be considered the official version of record. They are accessible to all readers and citable by the Digital Object Identifier (DOI®). “Just Accepted” is an optional service offered to authors. Therefore, the “Just Accepted” Web site may not include all articles that will be published in the journal. After a manuscript is technically edited and formatted, it will be removed from the “Just Accepted” Web site and published as an ASAP article. Note that technical editing may introduce minor changes to the manuscript text and/or graphics which could affect content, and all legal disclaimers and ethical guidelines that apply to the journal pertain. ACS cannot be held responsible for errors or consequences arising from the use of information contained in these “Just Accepted” manuscripts.

Theoretical and Shock Tube Study of the Rate Constants for Hydrogen

Abstraction Reactions of Ethyl Formate

Junjun Wu^a, Fethi Khaled^b, Hongbo Ning^a, Liuhaio Ma^a, Aamir Farooq^b, and Wei Ren^{a, c, *}

^a Department of Mechanical and Automation Engineering, The Chinese University of Hong Kong, New Territories, Hong Kong

^b King Abdullah University of Science and Technology (KAUST), Clean Combustion Research Center, Physical Sciences and Engineering Division, Thuwal 23955, Saudi Arabia

^c Shenzhen Research Institute, The Chinese University of Hong Kong, New Territories, Hong Kong

* Corresponding author. Fax: +852 2603 6002. Email: renwei@mae.cuhk.edu.hk (W. Ren)

Abstract:

We report a systematic chemical kinetics study of the H-atom abstractions from ethyl formate (EF) by H, O(³P), CH₃, OH, and HO₂ radicals. The geometry optimization and frequency calculation of all the species were conducted using the M06 method and the cc-pVTZ basis set. The one-dimensional hindered rotor treatment of the reactants and transition states and the intrinsic reaction coordinate analysis were also performed at the M06/cc-pVTZ level of theory. The relative electronic energies were calculated at the CCSD(T)/cc-pVXZ (where X = D, T) level of theory and further extrapolated to the complete basis set limit. Rate constants for the title reactions were calculated over the temperature range of 500–2500 K by the transition state theory (TST) in conjunction with asymmetric Eckart tunneling effect. In addition, the rate constants of H-abstraction by hydroxyl radical were measured in shock tube experiments at 900–1321 K and 1.4–2.0 atm. Our theoretical rate constants of OH + EF → Products agree well with the experimental results within 15% over the experimental temperature range of 900–1321 K. Branching ratios for the five types of H-abstraction reactions were also determined from their individual site-specific rate constants.

1. Introduction

Biodiesel has received intensive attention as it allows powering the world sustainably and cutting CO₂ debt potentially.¹⁻³ The typical compositions of biodiesel include fatty acid methyl esters (FAMES) and fatty acid ethyl esters (FAEEs),⁴ which are produced through esterification between alkyl alcohols and carboxylic acids. The current biodiesel production is almost monopolized in the form of FAMES since methanol, the key feedstock for FAMES, is well commercialized.⁵ However, there is a growing interest in the use of FAEE in biodiesel due to the safety concern of methanol.⁶ In the downstream, FAEEs have been tested in engines to show similar performance as the traditional diesel and FAMES, and emit even fewer pollutants.^{7,8} The utilization of FAEEs in transportation is foreseeable.

Ethyl formate (EF, HCOOC₂H₅) is the simplest surrogate in the large family of FAEEs. In fact, EF acts not only as the surrogate for FAEEs, but also presents as an important atmospheric pollutant. The gas-phase reactions of EF with chloride were studied to understand its atmospheric oxidation behavior.^{9,10} Moreover, EF is a compelling interstellar molecule firstly detected in the interstellar space in 2009,¹¹ leading to the investigation of unimolecular decomposition reactions of EF to understand the interstellar chemistry.^{12,13} Considering the prominence of EF in combustion, atmospheric and interstellar chemistry, it is thus selected as the target FAEE in this study with special emphasis on its combustion chemical kinetics.

The pyrolysis or oxidation of EF is initiated by unimolecular decomposition and hydrogen abstraction reactions. Regarding the pyrolysis of EF, Makens et al.¹⁴ conducted thermal decomposition experiments of EF at 500–700 K and discovered the principal decomposition pathway $\text{EF} \rightarrow \text{C}_2\text{H}_4 + \text{HCOOH}$. This finding was further confirmed by Blades^{15,16} using a flow

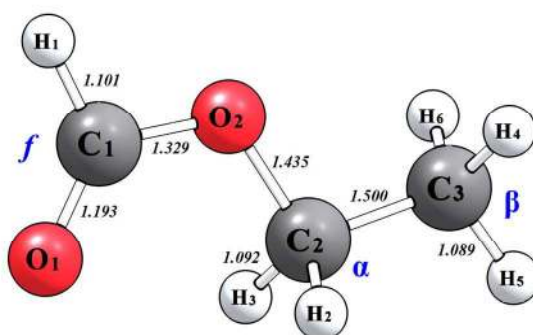
1
2
3 reactor at 830–903 K and Balaganesh et al.¹⁷ using a shock tube at 909–1258 K. This dominant
4
5 EF unimolecular reaction was theoretically studied by Hermida-Ramon et al.¹⁸ with the *ab initio*
6
7 and DFT methods at different levels of theory. Ren et al.¹⁹ recently reported the concentration
8
9 time-histories of CO, CO₂, and H₂O during the pyrolysis of EF in a shock tube, and performed
10
11 detailed chemical kinetic modeling analysis using the Westbrook et al. mechanism.²⁰
12
13
14

15
16 Regarding EF oxidation, Osswald et al.²¹ studied the destruction pathways of EF in laminar
17
18 flat flames and compared the oxidation products with methyl acetate (MA). The prevailing
19
20 intermediate of EF was found to be acetaldehyde while that for MA was formaldehyde.
21
22 Westbrook et al.²⁰ proposed the first reaction mechanism of EF with the rate constants for
23
24 unimolecular decomposition and H-abstraction reactions estimated from propane and methyl
25
26 cyclohexane using the principle of similarity.^{22,23} Benjamin et al.²⁴ measured the ignition delay
27
28 times of EF in a shock tube and found that the EF mechanism captured the major tendency but
29
30 somehow underestimated the ignition delay times at low pressures. A follow-up research by the
31
32 same group²⁵ developed a new EF mechanism tailored for predicting the high-temperature
33
34 ignition delay times, whereas the rate constants for the preliminary reactions of EF were
35
36 estimated analogically from propane.²⁶
37
38
39
40
41

42
43 It is evident from the above literature survey that, (i) there is still a need to revisit these rate
44
45 constants of EF reactions for more accurate chemical kinetic models, and (ii) the bimolecular H-
46
47 abstraction reactions of EF received less attention both theoretically and experimentally. To our
48
49 knowledge, only Wang et al.²⁷ calculated the rate constants for H-abstraction reactions of EF by
50
51 hydrogen radical at the CCSD(T)/CBS//B3LYP/6-311G(d,p) level of theory. To date, theoretical
52
53 calculations for the H-abstractions of EF by O (³P), CH₃, OH, and HO₂ have never been reported.
54
55
56 Hence, this work aims to provide a complete study of the rate constants for the H-abstractions of
57
58
59
60

1
2
3 EF by different radicals using the *ab initio* approach. In particular, the overall rate constant of
4
5 OH + EF was measured in shock tube experiments to further validate our theoretical calculations.
6
7
8 This study provides a consolidated foundation for the reaction mechanism development of EF
9
10 and other ethyl esters.
11

12 13 14 2. Computational details 15



31 **Figure 1.** Configuration of EF with the lowest energy.
32

33
34 Figure 1 shows the configuration of the most stable EF conformation that was identified by
35 scanning the three internal rotors (C_1-O_2 , O_2-C_2 and C_2-C_3) at the M06/cc-pVTZ level. Note
36 that EF has a planar skeleton constituted by atoms C_1 , H_1 , O_1 , O_2 , C_2 , C_3 and H_5 . These atoms
37 also form a mirror plane and thus EF belongs to C_s group. The hydrogen atoms of EF can be
38 divided into three groups according to their positions: H_1 in ester moiety, the identical H_2 and H_3
39 in methylene moiety, and H_4 , H_5 and H_6 in methyl moiety. Although H_5 is not rigorously
40 equivalent to H_4 and H_6 atoms, the energy differences of their transition states of H-abstraction
41 reactions are almost negligible (< 0.2 kcal/mol). Hence, it is reasonable to treat H_4 , H_5 and H_6 as
42 identical.
43
44
45
46
47
48
49
50
51
52
53
54
55
56
57
58
59
60

Based on the different carbon sites, the H-abstraction reactions of EF proceed through the following three channels:



where $\text{R}\cdot$ stands for radicals such as H, O (^3P), CH_3 , OH, and HO_2 . Ra, Rb, Rc are reactions with the H atom abstracted from formate group, α -carbon, and β -carbon, respectively (see Figure 1). Here, the formed three radicals from EF such as $\text{COOCH}_2\text{CH}_3$, HCOOCHCH_3 and $\text{HCOOCH}_2\text{CH}_2$ are denoted as EF·A, EF·B and EF·C, respectively. The optimized structures of these species are provided in Supporting Information. Note that radical EF·A presents an extended π -resonance involving C_1 , O_1 and O_2 , and EF·B also induces a stronger extended π -resonance involving C_1 , O_1 , C_2 and O_2 . In contrast, radical EF·C is formed without the π -resonance. As a result, TSb is expected to lie in the lowest energy while TSc in the highest energy. This is also consistent with the bond dissociation energy (BDE) calculation at the CCSD(T)/CBS(D-T)//M06/cc-pVTZ level of theory. Note that the BDEs for $\text{C}_1\text{-H}_1$, $\text{C}_2\text{-H}_{2/3}$, $\text{C}_3\text{-H}_{4/5/6}$ were calculated to be 98.6, 97.5 and 102.0 kcal/mol, respectively.

2.1 Potential energy surface

The DFT method hybrid exchange-correlation functional M06²⁸ with cc-pVTZ basis set was used for the geometry optimization and vibrational frequency calculation in Gaussian 09.²⁹ The close-shell species and open-shell species were treated by the restricted and unrestricted DFT methods, respectively. To locate the transition state (TS), a single imaginary frequency associated with the proper vibration mode is mandatory. Intrinsic reaction coordinate (IRC)

1
2
3 analysis was performed to ensure the TS connects the right reactants and products. Particularly
4
5 for the H-abstraction reactions by OH and HO₂, the H-bonding between H atoms and O atoms
6
7 emerges to form both reactant and product complexes. These complexes were captured by the
8
9 further optimization at the M06/cc-pVTZ level on the reactant and product ends of IRC. A
10
11 scaling factor of 0.998 for frequency correction and 0.984 for zero point energy (ZPE) correction
12
13 were used in our calculations.³⁰
14
15
16

17
18 The single-reference method CCSD(T) with the basis set of cc-pVXZ (X=D, T) was
19
20 employed to obtain more reliable energies. The T_1 diagnostic values (See Supporting Information)
21
22 of CCSD(T) calculations were found generally less than the criteria 0.02,³¹ except for the TSs of
23
24 reactions $O + EF \rightarrow OCOC_2H_5 + OH$ and $OH + EF \rightarrow OCOC_2H_5 + H_2O$, with T_1 values of 0.022
25
26 and 0.023, respectively. Nevertheless, an empirical threshold T_1 value of 0.04 was recommended
27
28 for open-shell species.³² Hence, despite the slightly higher T_1 values, the energies of these two
29
30 TSs can also be safely computed with the single-reference method. Finally, the two-point
31
32 extrapolation scheme³³ was adopted for complete basis set (CBS) limit energies E_∞ :
33
34
35
36

$$E(l_{max}) = E_\infty + \frac{B}{(l_{max}+1)^4} \quad (\text{Eqn. 1})$$

37
38 where l_{max} is the maximum angular momentum function within the three basis sets, and B is the
39
40 system-specific parameter. With this scheme, the energy extrapolated to the CBS limit using
41
42 single point calculations by cc-pVDZ and cc-pVTZ basis sets was adopted in this work, denoted
43
44 as CCSD(T)/CBS(D-T).
45
46
47
48
49
50

51 52 2.2 Rate constant calculation

53
54 Rate constants for all the H-abstraction reactions were calculated with tight transition state
55
56 theory (TST) in KisThelP program.³⁴ Reactions OH/HO₂ + EF proceed through a three-step
57
58
59
60

1
2
3 scheme (*vide infra*) due to the formation of reactant and product H-bond complexes. However,
4 these H-bond complexes are only of kinetic importance at very low temperatures. Thus it is
5 justified to treat OH/HO₂ + EF reactions with TST over the temperature range of 500–2500 K.
6
7
8
9

10
11 One-dimensional (1D) hindered rotor approximation was considered for the low-frequency
12 torsional modes. The hindrance potentials of the involved species were obtained using the
13 relaxed scan by a dihedral angle step of 10° at the M06/cc-pVTZ level of theory. For the
14 transition states, 1D rotor scans were performed by freezing the atoms involved in the reaction
15 coordinate. In addition, the asymmetric Eckart tunneling correction³⁵ was applied and the final
16 rate constants were obtained by:
17
18
19
20
21
22
23

$$k^{TST}(T) = \chi(T) \cdot \sigma \frac{k_b T}{h} \frac{Q^{TS}(T)}{Q^R(T)} \text{Exp} \left(-\frac{V^{++}}{k_b T} \right) \quad (\text{Eqn. 2})$$

24
25
26
27
28
29
30 where $\chi(T)$ is the asymmetric Eckart tunneling correction coefficient, σ is the reaction path
31 degeneracy, k_b is the Boltzmann's constant, T is the temperature, h is the Planck's constant,
32 $Q^{TS}(T)$ is the partition function of the transition state, $Q^R(T)$ is the partition function of the
33 reactants, and V^{++} represents the activation energy of the considered reaction. Finally, the rate
34 constants obtained at 500–2500 K were further fitted to the three-parameter modified Arrhenius
35 equation:
36
37
38
39
40
41
42
43
44

$$k(T) = AT^n \exp\left(-\frac{E_a}{RT}\right). \quad (\text{Eqn. 3})$$

45 46 47 48 49 **3. Shock tube/laser absorption experiment**

50
51
52 The rate constant measurements of EF with hydroxyl radical (EF + OH → Products) were
53 carried out behind the reflected shock wave in the low-pressure shock tube facility at King
54 Abdullah University of Science and Technology (KAUST). The rate of progress of the reaction
55
56
57
58
59
60

1
2
3 was followed by monitoring the OH concentration time profile. Hydroxyl radicals were detected
4
5 at the $R_1(5)$ rovibrational transition of the $A-X(0,0)$ electronic system near 306.7 nm using a
6
7 narrow-linewidth (< 200 kHz) continuous wave UV laser source. Details about the shock tube
8
9 and the laser system can be found elsewhere;³⁶ only brief description is given here. Laser
10
11 absorption diagnostics for the other radicals such as H/O atoms, CH_3 , OH, and HO_2 radicals are
12
13 currently not available for shock tube experiments. Here we only report the measured rate
14
15 constants of EF with hydroxyl radical.
16
17
18

19
20 The shock tube is composed of a 9 m long driven section, and the driver section length can
21
22 be varied to a maximum of 9 m depending on the required test times. The diameter of the shock
23
24 tube is 14.2 cm. The shock tube driven section was evacuated before each experiment with a
25
26 turbo-molecular pump to a pressure of about 1×10^{-5} Torr to eliminate impurities. *Tert*-butyl
27
28 hydroperoxide (TBHP) was chosen as thermal precursor for OH radicals in this study since it
29
30 decomposes very rapidly (less than 10 μs at $T > 800$ K; less than 1 μs at $T > 1100$ K) to produce
31
32 OH and other less reactive radicals.³⁷ A mixture of 309 ppm ethyl formate and 20 ppm TBHP in
33
34 argon was prepared in a mixing vessel equipped with turbo-molecular vacuum pump and a
35
36 magnet mixing stirrer. The mixture was left to homogenize for at least 2 hours prior to use in
37
38 shock tube experiments. The TBHP aqueous solution (70% TBHP/30% H_2O) and ethyl formate
39
40 ($>97\%$ purity) were obtained from Sigma-Aldrich. Incident shock velocity measurements were
41
42 carried out using five PZT pressure transducers (PCB 113B26) placed over the last 1.5 m of the
43
44 driven section of the shock tube. The pre-shock pressure (P_1) in the driven section was measured
45
46 using two high-accuracy Baratron pressure transducers. Temperature and pressure behind
47
48 reflected shock waves (T_5 and P_5) were determined using the standard shock-jump relations³⁸
49
50 with the measured incident shock speed and known thermodynamic parameters as inputs.
51
52
53
54
55
56
57
58
59
60

1
2
3 The UV beam (~ 50 mW) was generated by frequency doubling the red beam near 613.4 nm
4
5 (~ 1 W) generated by a cw ring-dye laser that was pumped by an Nd:YAG at 532 nm (~ 10 W).
6
7 A wave-meter (Bristol 610) was used to monitor the visible laser wavelength. To minimize the
8
9 noise caused by laser intensity fluctuations, common-mode-rejection scheme was applied by
10
11 splitting the UV beam with a beam splitter prior to the shock tube. Beer-Lambert law, $I/I_0 =$
12
13 $\exp(-k_{\text{OH}}X_{\text{OH}}PL)$, was used to convert the measured signal to absolute OH concentration, where I
14
15 and I_0 are the transmitted and incident laser intensities, k_{OH} is the OH absorption coefficient, X_{OH}
16
17 is the OH mole fraction, P is the total pressure (atm), and L is the path length (14.2 cm). The
18
19 estimated uncertainty in the measured OH mole fraction (X_{OH}) is approximately $\pm 3\%$, mainly
20
21 due to the uncertainties in the reflected-shock temperature and hydroxyl absorption coefficient.³⁹⁻
22
23
24
25
26

27 ⁴⁰ The minimum detectable hydroxyl mole fraction is less than 1 ppm.
28
29

30 **4. Results and discussion**

31
32

33 All the H-abstractions can be divided into two categories, one category involves H/O/CH₃ +
34
35 EF reactions to be discussed in Section 4.1, and the other category OH/HO₂ + EF with H-bond
36
37 complexes to be discussed in Section 4.2.
38
39

40 **4.1 H/O/CH₃ + EF reactions**

41
42

43 **4.1.1 Structures & energies**

44
45

46 Considering the similarity of H/O/CH₃ + EF reactions, only the structures and energies for H
47
48 + EF are discussed here. Details for all these three types of reactions are provided in Supporting
49
50 Information.
51
52

53
54 Figure 2 depicts the optimized structures of TSs for H + EF reactions. The C–H and H–H
55
56 bonds undergoing bond breaking and forming are critical for the TS formation. The
57
58
59
60

corresponding bond lengths and angles are calculated and compared with those obtained at the B3LYP/6-311G(d, p) level.²⁷ The discrepancies of structures (including bond length and angle) obtained at these two levels of theory are within 2% for TSa and TSb, whereas the difference ranges between 5% and 8% for TSc. We expect such a larger difference of structure on TSc may cause a non-negligible difference in the energy barriers.

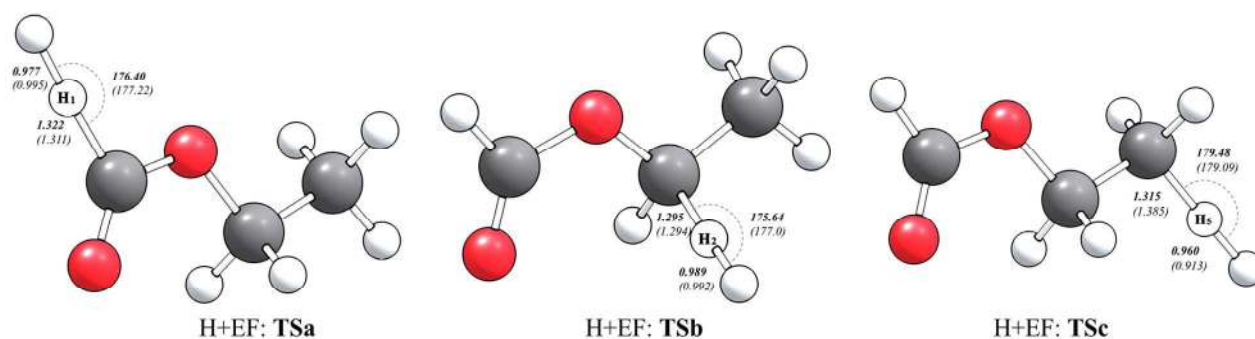


Figure 2. Optimized geometries (Ångstrom and degree) of TSs for H + EF reaction at the M06/cc-pVTZ level. In brackets are the structures optimized at the B3LYP/6-311G(d, p) level.²⁷ TSa, TSb and TSc are the transition states associated with reactions to produce radicals EF·A, EF·B and EF·C, respectively.

Figure 3 depicts the ZPE-corrected relative energies of TSs and products obtained at different theory levels. For transition states TSa and TSb, the energy barriers derived from CCSD(T)/CBS(D-T)/M06/cc-pVTZ used in this work and CCSD(T)/CBS(D-T-Q)/B3LYP/6-311G(d,p) used in the previous study²⁷ only differ by 0.1 kcal/mol. However, this difference increases to 1.2 kcal/mol for TSc, which is analyzed primarily due to the geometry deviation between these two methods. This observation implies that TSc is more susceptible to the choice of basis sets. We used another smaller basis set, i.e. 6-31G(d,p), to optimize the structures of all the aforementioned species. Energies obtained at the CCSD(T)/cc-pVDZ and CCSD(T)/cc-pVTZ levels were extrapolated to the CCSD(T)/CBS(D-T) level. We observed that the energies for TSc differ by ~1.0 kcal/mol between the CCSD(T)/CBS(D-T)/M06/cc-pVTZ and CCSD(T)/CBS(D-

T)//M06/6-31G(d,p) levels. A higher basis set provides more accurate geometries for TSs¹⁸ and potentially reduces the superposition errors in the energy extrapolation.⁴¹ Hence, the CCSD(T)/CBS(D-T)//M06/cc-pVTZ method was preferred throughout this work.

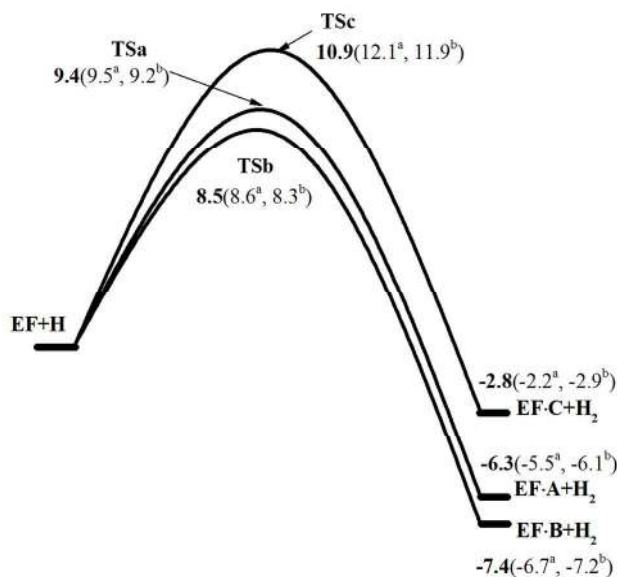


Figure 3. ZPE-corrected PESs for H + EF reactions (energy in kcal·mol⁻¹). Numbers in bold are relative energies obtained at the CCSD(T)/CBS(D-T)//M06/cc-pVTZ level, energies with the superscript-a in brackets were obtained at the CCSD(T)/CBD(D-T-Q)//B3LYP/6-311G(d, p) level,²⁷ and energies with the superscript-b in brackets were obtained at the CCSD(T)/CBD(D-T)//M06/6-31G(d, p) level.

4.1.2 Rate constant & branching ratio

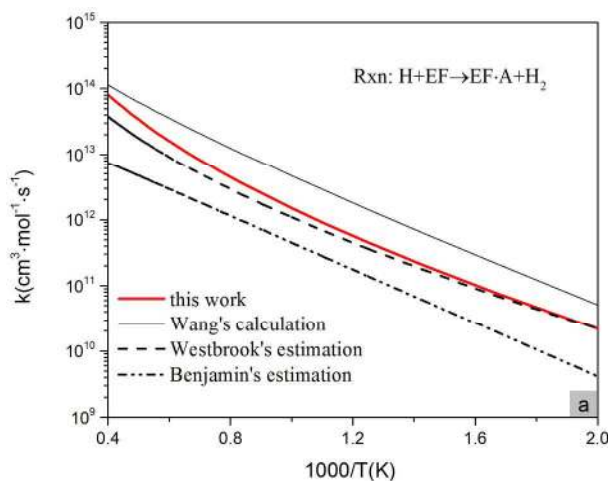
The bimolecular rate constants were computed using the conventional TST with 1D hindered rotor approximation. These rate constants obtained over the temperature range of 500–2500 K are further fitted to the modified Arrhenius equation. Table 1 lists all the site-specific rate constants for H-abstraction reactions of EF by H, O(³P) and CH₃ radicals.

Table 1. Site-specific H-abstraction rate constants for H/O/CH₃ + EF reactions.

Reaction	$A/\text{cm}^3 \cdot \text{mol}^{-1} \cdot \text{s}^{-1}$	n	$E/\text{kcal} \cdot \text{mol}^{-1}$
H + EF → EF·A + H ₂	2.97×10^4	2.89	4.43
H + EF → EF·B + H ₂	3.97×10^4	2.78	3.77
H + EF → EF·C + H ₂	2.21×10^4	3.17	5.10
O + EF → EF·A + OH	1.56×10^5	2.69	4.45
O + EF → EF·B + OH	7.21×10^4	2.73	3.66
O + EF → EF·C + OH	6.32×10^3	3.04	5.79
CH ₃ + EF → EF·A + CH ₄	4.63×10^{-3}	4.29	7.25
CH ₃ + EF → EF·B + CH ₄	2.66×10^{-3}	4.32	6.77
CH ₃ + EF → EF·C + CH ₄	1.63×10^{-2}	4.22	10.23

Figure 4 compares the rate constants of H + EF reactions determined in this study with the previous calculations by Wang et al.²⁷ and the estimated values by Westbrook et al.²⁰ and Benjamin et al.²⁵ For reaction H + EF → EF·A + H₂, according to our previous discussion, the energy barriers calculated at the CCSD(T)/CBS(D-T)//M06/cc-pVTZ and CCSD(T)/CBS(D-T-Q)//B3LYP/6-311G(d,p) levels are almost identical, implying that the rate constants may be similar at these two levels of theory. However, as shown in Figure 4a, our rate constants are lower than Wang's calculations²⁷ by a factor of 1.4–3.2. Note that we considered the hindered rotors of all species in this study, which were ignored in the calculations by Wang et al.²⁷

1
2
3 Additionally, Westbrook's estimations²⁰ agree very well with our calculations, which fall into the
4 uncertainty region of $\pm 50\%$ of our results. Similarly, for reaction $\text{H} + \text{EF} \rightarrow \text{EF}\cdot\text{B} + \text{H}_2$, Wang's
5 predictions²⁷ are still higher than our calculations by a factor of 2.0–3.7, whereas Westbrook's
6 estimations²⁰ are about 2 times lower than our results shown in Figure 4b. However, compared
7 with our calculations, Benjamin et al.²⁵ estimated lower rate constants for reaction Ra by a factor
8 of 5–10, and higher rate constants for reaction Rb by a factor of 2–19. Finally, for reaction $\text{H} +$
9 $\text{EF} \rightarrow \text{EF}\cdot\text{C} + \text{H}_2$, our calculations agree well with Wang's results²⁷ at higher temperatures, but
10 differ by a factor of 3 at lower temperatures (< 600 K). It is also seen that Benjamin's
11 estimations²⁵ are very close to our calculations particularly in the temperature range of 500–1600
12 K (Figure 4c).



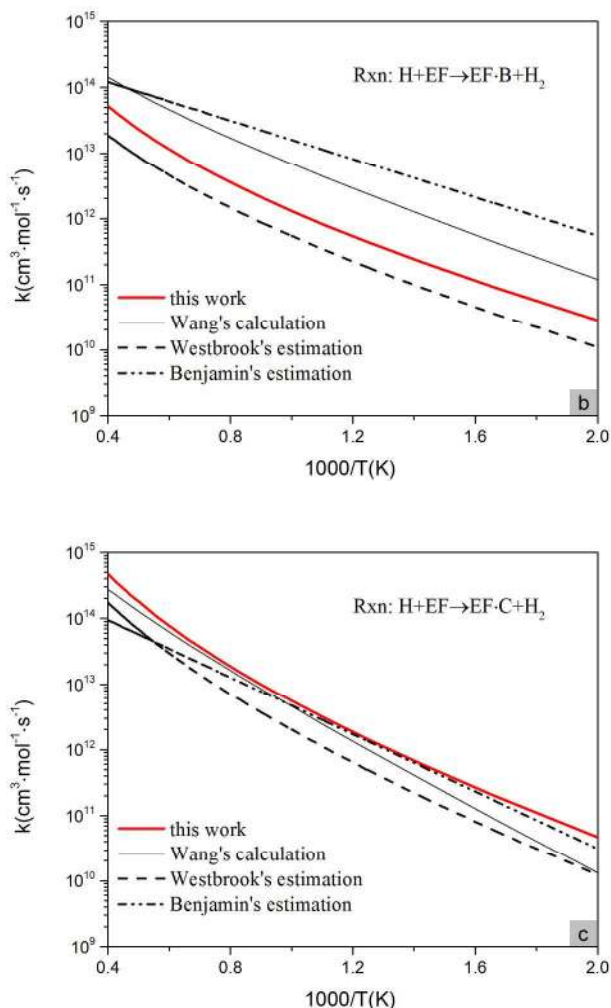


Figure 4. Comparison of the calculated rate constants for $\text{H} + \text{EF} \rightarrow$ products: (a) $\text{H} + \text{EF} \rightarrow \text{EF} \cdot \text{A} + \text{H}_2$, (b) $\text{H} + \text{EF} \rightarrow \text{EF} \cdot \text{B} + \text{H}_2$, and (c) $\text{H} + \text{EF} \rightarrow \text{EF} \cdot \text{C} + \text{H}_2$.

The site-specific rate constants for the H-abstraction reactions of EF by O and CH_3 are provided in the Supporting Information. Here we only plot the overall rate constants of these reactions in Figure 5 for comparison. In general, the reaction $\text{CH}_3 + \text{EF} \rightarrow$ Products possess the lowest rate constant, which is mainly due to the large energy barriers ranging from 12.7 to 15.7 kcal/mol. Our calculations are lower than the estimated values by Westbrook et al.²⁰ and Benjamin et al.²⁵ particularly at lower temperatures. The rate constants of $\text{H} + \text{EF}$ and $\text{O} + \text{EF}$ are quite close at low temperatures but differ by a factor of 2–3 at higher temperatures (1100–2500

K). It is of interest to see that the rate constants of H + EF are always larger than those of O + EF, which is not consistent with their energy barriers. The energy barriers of O + EF at those three carbon sites are consistently lower than those of H + EF by ~ 2 kcal/mol.

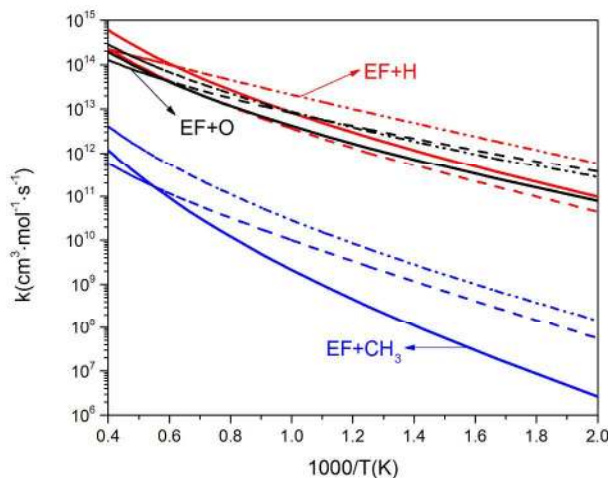


Figure 5. Overall rate constants for H-abstractions of EF by H (red), O (black), and CH₃ (blue). The rate constants calculated in this work (solid line) are compared with those estimated by Westbrook (dashed line)²⁰ and Benjamin (dash-dot-dot line).²⁵

The branching ratio was obtained by taking the ratio of the site-specific rate constant to the overall rate constant. Figure 6 illustrates the calculated branching ratios of these three types of reactions over the temperature range of 500–2500 K. In general, reaction types Ra and Rb hold similar branching ratios for H/O/CH₃ + EF reactions, which is possibly because Ra and Rb have a very close energy barrier with a small difference of 0.2–0.9 kcal/mol. For H + EF reactions (Figure 6a), the dominant channel H + EF → EF·C + H₂ (Rc) has a branching ratio of 0.50 at 500 K and 0.80 at 2500 K. For O + EF reactions (Figure 6b), Ra and Rb dominate the hydrogen abstraction of EF with a branching ratio of 0.40–0.50 and 0.30–0.60, respectively. In comparison, all Ra, Rb and Rc have similar branching ratios for CH₃ + EF reactions at higher temperatures

(2000–2500 K), but R_c decreases significantly at lower temperatures. For instance, at 500 K, R_c has a branching ratio of 0.05, compared with 0.45 for R_a and 0.50 for R_b (Figure 6c).

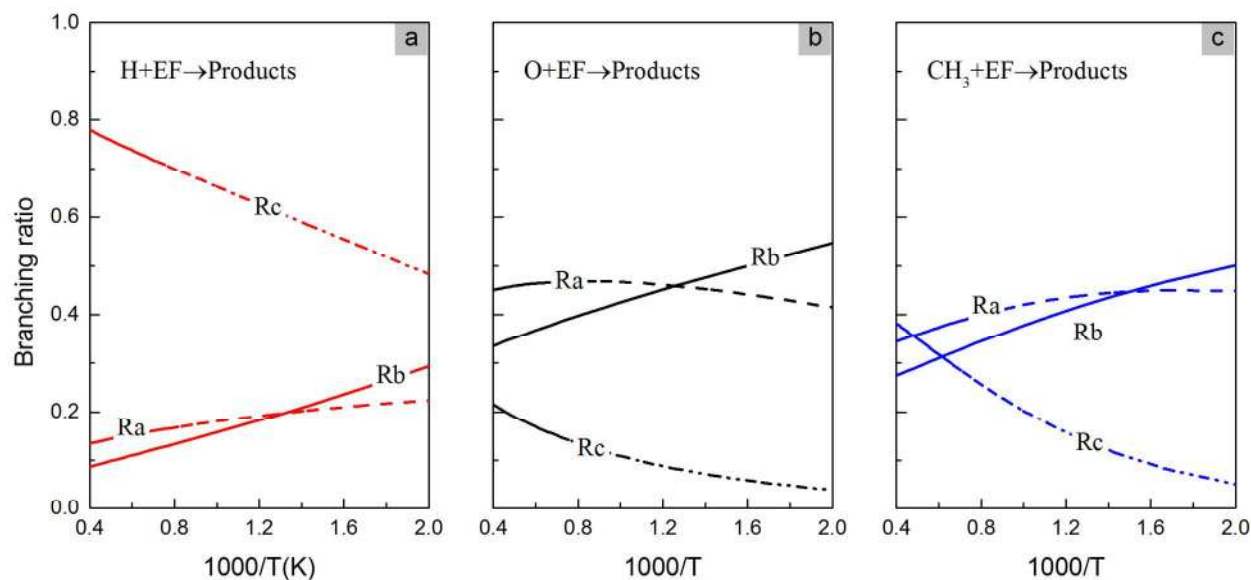


Figure 6. Branching ratios for the three H-abstraction channels: (a) $H + EF \rightarrow \text{Products}$, (b) $O + EF \rightarrow \text{Products}$, and (c) $CH_3 + EF \rightarrow \text{Products}$.

4.2 OH/HO₂ + EF reactions

4.2.1 Structures & energies

Different from $H/O/CH_3 + EF$ reactions, the H atom in OH/HO₂ and O atoms in EF interact via the weak H-bonds leading to the different reaction schemes. The H atoms are abstracted via a three-step process: (1) OH/HO₂ combines with EF to form the reactant complexes (RCs), (2) RCs convert to product complexes (PCs) via TS, and (3) PCs decompose to EF radicals and H₂O/H₂O₂. Note that the RCs and PCs are formed via H-bonds and all these H-bond complexes are quite unstable especially at high temperatures.

Figure 7 exhibits the optimized structures of RCs, TSs and PCs for OH + EF reactions. It is seen that RCs have two or three H-bonds. These H-bond lengths are 2.0–2.1 Å except for RCb

with a shorter H-bond length of 1.916 Å. Conceptually, RCb with a shorter H-bond is more energetically stable than RCa and RCb. Additionally, the forming O–H bonds for the TSs are consistently longer than the breaking C–H bonds, indicating the early TSs. For all those three PCs, only one H-bond is formed for each reaction and thus PCs are less stable compared with RCs.

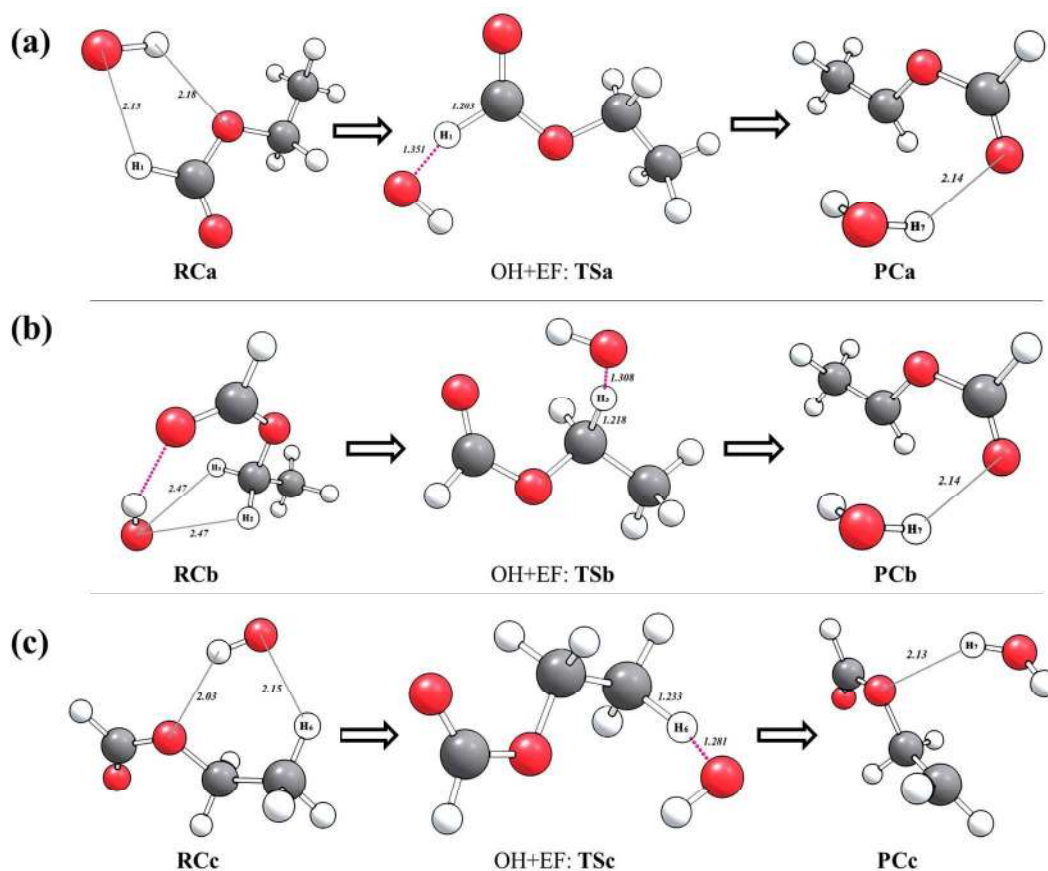
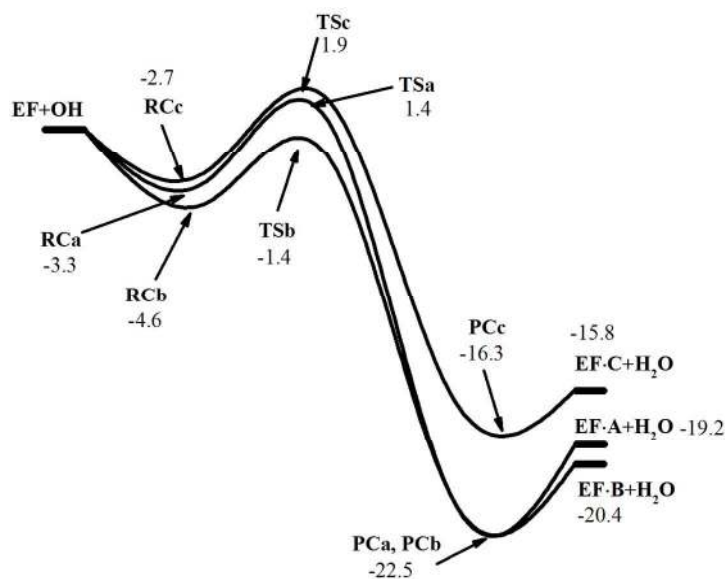


Figure 7. Optimized structures of reactant complexes, TSs and product complexes at the M06/cc-pVTZ level for OH + EF reactions: (a) $\text{OH} + \text{EF} \rightarrow \text{EF}\cdot\text{A} + \text{H}_2\text{O}$, (b) $\text{OH} + \text{EF} \rightarrow \text{EF}\cdot\text{B} + \text{H}_2\text{O}$, and (c) $\text{OH} + \text{EF} \rightarrow \text{EF}\cdot\text{C} + \text{H}_2\text{O}$. Bond lengths are given in Ångstroms.

Figure 8 shows the PESs for $\text{OH} + \text{EF} \rightarrow \text{Products}$ obtained at the CCSD(T)/CBS(D-T)//M06/cc-pVTZ level of theory. Two extra potential wells are seen for each PES due to the presence of H-bond complexes. The three RCs have a well depth of 2.7–4.6 kcal/mol relative to

1
2
3 the reactants. Particularly RCb holds a relative energy of -4.6 kcal/mol, which is 1.3 and 1.9
4 kcal/mol lower than that of RCa and RCc, respectively. Such a difference is consistent with our
5 previous structure analysis that RCb is energetically more stable than RCa and RCc. The relative
6 energies of TSs range from -1.4 kcal/mol to 1.9 kcal/mol, which are distinctly lower than those
7 of H/O/CH₃ + EF reactions. The lower energies indicate that EF and hydroxyl may react much
8 faster than H/O/CH₃ + EF reactions. In addition, Figure 8 demonstrates a well depth of 1.5–3.3
9 kcal/mol for the PCs relative to their corresponding products. The shallower wells imposed by
10 PCs compared to RCs imply that PCs are less important in H-abstraction reactions compared
11 with RCs. It is of interest to know how these H-bond complexes affect the H-abstraction
12 reactions. The energy barriers for RCs → EF + OH vary from 2.7 to 4.6 kcal/mol, which are
13 comparable with the energy barriers for RCs → TSs (3.0 to 4.7 kcal/mol). The similar barrier
14 heights of the two competing pathways indicate that RCs should be carefully considered when
15 calculating the overall rate constant of H-abstraction (*vide infra*). In contrast, the energy barriers
16 for PCs → Products are 1.5–3.3 kcal/mol, dramatically lower than that for PCs → TSs (18.2–
17 23.9 kcal/mol). Therefore, the contribution of PCs to the overall rate constant is negligible.



1
2
3 **Figure 8.** ZPE-corrected PESs for OH + EF reactions at the CCSD(T)/CBS(D-T)//M06/cc-pVTZ level (energy in
4 kcal·mol⁻¹).
5
6
7

8 Similarly, the detailed structures and PESs for HO₂ + EF → Products are provided in
9 Supporting Information. It is noteworthy that the TSs of HO₂ + EF are closer to the products
10 leading to endothermic reactions, different from OH + EF reactions with the feature of
11 exothermicity. The energy barriers for HO₂ + EF range from 17.1 to 22.5 kcal/mol, higher than
12 H/O/CH₃/OH + EF reactions. Moreover, the high energy barrier of HO₂ + EF suggests a minor
13 contribution of RCs and PCs to the overall rate constant⁴¹ and thus the RCs and PCs can be fairly
14 ignored.
15
16
17
18
19
20
21
22
23

24 **4.2.2 Rate constant & branching ratio**

25
26
27
28 Two strategies are possibly applicable to obtain the rate constants for OH/HO₂ + EF reactions.
29 One method is to treat OH/HO₂ + EF as a two-step reaction involving (1) barrierless RC
30 formations, known as the outer TSs, and (2) H-abstraction via inner TSs to form products. Note
31 that the PCs are energetically negligible for the rate constant calculation. To this end, a two-TS
32 model is necessary to include the contribution of RCs to the overall rate constant, where VRC-
33 TST is applied to account for the OH/HO₂ + EF → RCs reaction and TST is considered for RCs
34 → Products. Previous studies⁴¹⁻⁴² adopting the two-step strategy identified that the outer TSs
35 only matter at very low temperatures (< 200 K). The inner TSs are rate-determining over the
36 temperature range of 500–2500 K. Alternatively, the TST method can be adopted to readily
37 calculate the rate constants for OH/HO₂ + EF, regardless of the RC formation. Such a
38 simplification is also kinetically robust since these weak H-bonds of RCs are rather unstable at
39 high temperatures. Hence, it is fairly justified to use the TST method for the rate constant
40 determination of OH/HO₂ + EF reactions in this study.
41
42
43
44
45
46
47
48
49
50
51
52
53
54
55
56
57
58
59
60

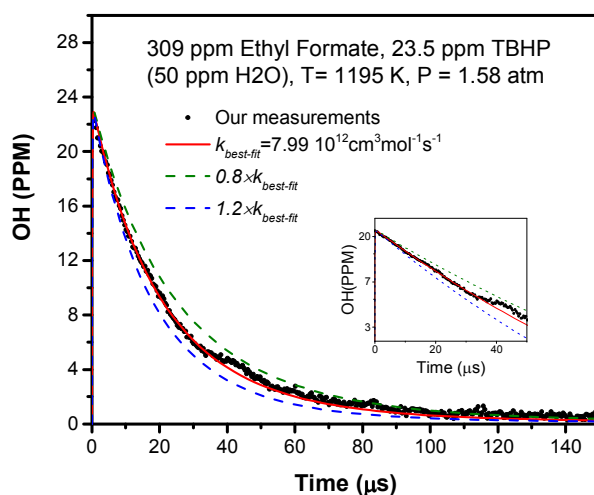
It should be pointed out that the Eckart tunneling correction is not applicable for $\text{OH} + \text{EF} \rightarrow \text{EA}\cdot\text{B} + \text{H}_2\text{O}$ (Rb) due to the negative energy barrier. Instead, we used the Winger method⁴³ to account for the tunneling effect. This is acceptable according to our calculations that the deviation between Eckart tunneling and Winger tunneling is around 6–20% over the temperature range of 500–2500 K. The calculated site-specific rate constants for $\text{OH}/\text{HO}_2 + \text{EF} \rightarrow \text{Products}$ are listed in Table 2. Detailed site-specific rate constants are compared with formic acid⁴⁴, methyl formate^{45,46}, ethyl acetate⁴⁷ and methyl propanoate⁴⁸ and provided in Supporting Information.

Table 2. Site-specific rate constants for $\text{OH}/\text{HO}_2 + \text{EF} \rightarrow \text{Products}$ at 500–2500 K.

Reaction	$A/\text{cm}^3\cdot\text{mol}^{-1}\cdot\text{s}^{-1}$	n	$E/\text{kcal}\cdot\text{mol}^{-1}$
$\text{OH} + \text{EF} \rightarrow \text{EF}\cdot\text{A} + \text{H}_2\text{O}$	2.76×10^3	2.94	-0.14
$\text{OH} + \text{EF} \rightarrow \text{EF}\cdot\text{B} + \text{H}_2\text{O}$	3.47×10^1	3.30	-4.28
$\text{OH} + \text{EF} \rightarrow \text{EF}\cdot\text{C} + \text{H}_2\text{O}$	3.32×10^3	2.80	-0.87
$\text{HO}_2 + \text{EF} \rightarrow \text{EF}\cdot\text{A} + \text{H}_2\text{O}_2$	4.69×10^{-2}	4.13	15.36
$\text{HO}_2 + \text{EF} \rightarrow \text{EF}\cdot\text{B} + \text{H}_2\text{O}_2$	1.81×10^{-3}	4.28	12.68
$\text{HO}_2 + \text{EF} \rightarrow \text{EF}\cdot\text{C} + \text{H}_2\text{O}_2$	3.52×10^{-2}	4.34	18.68

The calculated rate constants for $\text{EF} + \text{OH} \rightarrow \text{Products}$ are compared with the shock tube measurements conducted at 900–1321 K and 1.4–2.0 atm. A representative measured hydroxyl concentration profile is presented in Figure 9 for $\text{EF} + \text{OH}$ rate constant measurement. The black

1
2
3 trace shows high signal-to-noise ratio achieved for these measurements. To model the measured
4 hydroxyl profiles, a reaction mechanism was assembled which comprises of ethyl formate
5 chemistry by Metcalfe et al.⁴⁹ and TBHP chemistry by Pang et al.⁵⁰ The overall rate constant of
6 EF + OH \rightarrow Products was varied in the mechanism to achieve the best-fit to the measured OH
7 trace. The best-fit rate and perturbations of $\pm 20\%$ are plotted in Figure 9 as the representative
8 case. The reaction mechanism was used to perform hydroxyl sensitivity analysis which
9 highlights key reactions affecting the OH decay. A representative sensitivity analysis shown in
10 Figure 10 indicates that OH decay is primarily controlled by the reaction EF + OH \rightarrow Products.
11 Uncertainty in the rate constant measurement is estimated to be $\pm 15\%$, which primarily comes
12 from uncertainties in mixture composition, temperature, pressure and rate constants of secondary
13 interfering reactions. Table 3 summarizes the experimentally determined rate constants at
14 different temperatures and pressures.



50
51
52
53
54
55
56
57
58
59
60

Figure 9. Representative hydroxyl mole fraction time profile. Inset in log scale shows the linear decay of OH. Solid red line is the best-fit simulated profile and the dashed lines represent $\pm 20\%$ perturbations of the best-fit rate.

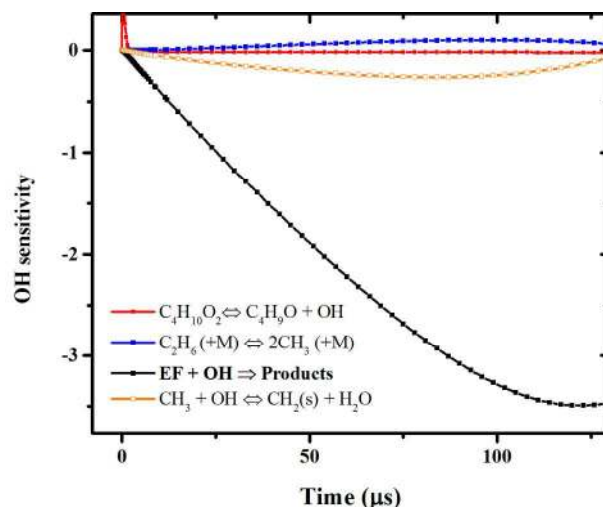


Figure 10. Hydroxyl sensitivity analysis for a mixture of 309 ppm EF and 23.5 ppm TBHP in argon at 1195 K and 1.58 atm. Sensitivity is defined here as $S = (\partial X_{\text{OH}}/\partial k_i) \times (k_i/X_{\text{OH}})$ where X_{OH} is the OH mole fraction and k_i is the rate constant of reaction i .

Table 3. Measured rate constants of $\text{EF} + \text{OH} \rightarrow \text{Products}$.

P /atm	T /K	k / $\text{cm}^3 \text{mol}^{-1} \text{s}^{-1}$
1.39	1321	1.24×10^{13}
1.48	1303	1.19×10^{13}
1.5	1222	9.01×10^{12}
1.58	1195	7.99×10^{12}
1.63	1113	6.69×10^{12}
1.68	1090	6.82×10^{12}
1.66	1028	5.84×10^{12}
1.78	984	5.42×10^{12}
2.18	939	5.18×10^{12}
1.76	907	4.99×10^{12}
2.04	900	4.95×10^{12}

Figure 11 compares our calculations of the overall rate constants for $\text{OH} + \text{EF} \rightarrow \text{Products}$ with the shock tube measurements (900–1300 K, 1.4–2.0 atm). Our calculations agree well with the experimental data (within 15%) over the experimental temperature range. Westbrook et al.'s estimations²⁰ agree with our calculations within 30% over the temperature range of 700–1800 K. Beyond this temperature range, the estimated values²⁰ are lower than our calculations by a factor of 1.3–1.9. However, the rate constants estimated by Benjamin et al.²⁵ from the OH + propane reactions are significantly lower (at least a factor of 8) than our calculations and the experimental results. Such a discrepancy is mainly due to the different C–H bond properties in propane and EF, as suggested by Westbrook et al.²⁰

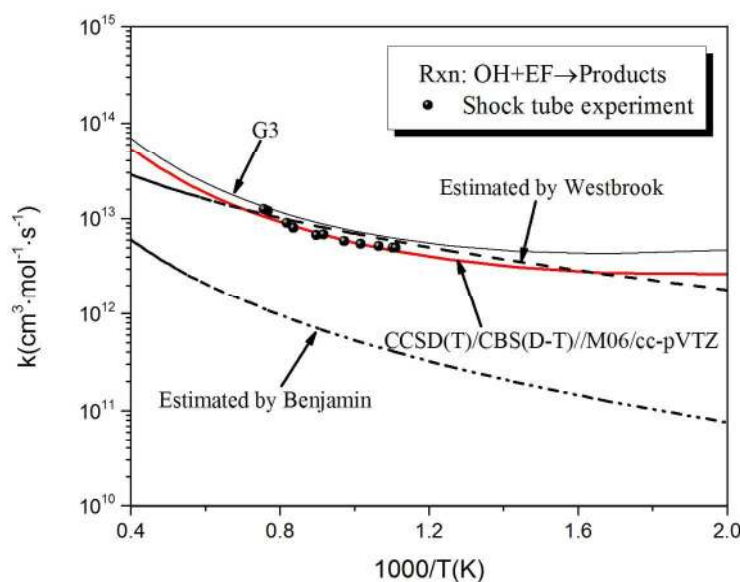


Figure 11. Comparison of the calculated rate constants of $\text{OH} + \text{EF} \rightarrow \text{Products}$ with shock tube experiments. Red line, calculation at the CCSD(T)/CBS(D-T)//M06/cc-pVTZ level (this work); thin solid line, calculation at the G3 level (this work); dashed line, estimation by Westbrook et al.²⁰; dash-dot-dot line, estimation by Benjamin et al.²⁵

In order to evaluate the uncertainty of our calculations, we used another composite method G3 to construct the PES and recalculated the rate constants accordingly; calculation details are provided in Supporting Information. The theoretical results at the G3 level are also plotted in

Figure 11 for comparison. The rate constants obtained at the G3 level have a very similar tendency to those calculated at the CCSD(T)/CBS(D-T)//M06/cc-pVTZ level, although the absolute values are slightly higher by a factor of 1.3–1.8.

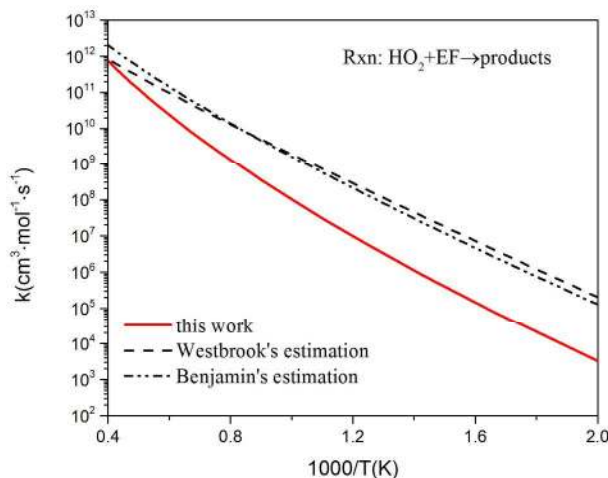


Figure 12. Comparison of rate constants for $\text{HO}_2 + \text{EF} \rightarrow \text{Products}$: red solid line, calculation at the CCSD(T)/CBS(D-T)//M06/cc-pVTZ level (this work); dashed line, estimation by Westbrook et al.²⁰; dash-dot-dot line, estimation by Benjamin et al.²⁵

The energy barriers of $\text{HO}_2 + \text{EF}$ reactions are much higher than that of $\text{OH} + \text{EF}$ reactions by 17.1 kcal/mol (Rb channel) to 22.5 kcal/mol (Rc channel). Such a high energy barrier acts as the bottleneck for the rate constant determination rather than the H-bond complexes. Thus contributions of these H-bond complexes to the final rate constants can be safely neglected. Figure 12 compares the overall rate constants calculated in this work with the estimations by Westbrook et al.²⁰ and Benjamin et al.²⁵ These estimations are higher than our calculations, particularly at lower temperatures. Note that both estimations were derived from the abstraction reactions of $\text{HO}_2 + \text{propane}$.²⁶

Finally, we plot the branching ratios of all the channels of $\text{OH}/\text{HO}_2 + \text{EF}$ shown in Figure 13. For $\text{OH} + \text{EF}$ reactions, reaction type Rb presents as the dominant channel with a branching ratio

of 0.4–0.8 over the temperature range of 500–1200 K. At higher temperatures (1300–2500 K), Rb and Rc have very similar branching ratios of ~ 0.25 , whereas Ra dominates with a branching ratio of ~ 0.5 . In comparison, Ra always holds a considerable branching ratio of 0.3–0.5 for $\text{HO}_2 + \text{EF}$ reactions over the entire temperature range of 500–2500 K. At lower temperatures (500–650 K), Rb has a branching ratio of 0.5–0.6 compared with the negligible branching ratio (< 0.1) for Rc. However, at higher temperatures (1500–2500 K), Rc becomes dominant with a branching ratio of 0.5–0.6, whereas Rb shows very little influence on $\text{HO}_2 + \text{EF}$ reaction.

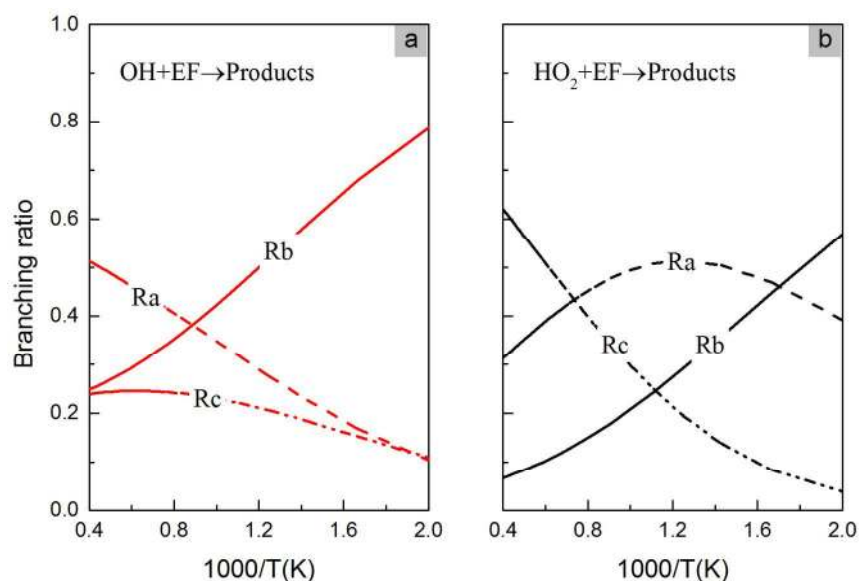


Figure 13. Branching ratios for the $\text{OH}/\text{HO}_2 + \text{EF}$ reactions: (a) $\text{OH} + \text{EF} \rightarrow \text{Products}$, and (b) $\text{HO}_2 + \text{EF} \rightarrow \text{Products}$.

5. Conclusions

The H-abstraction reactions of EF by different radicals (H, O (^3P), CH_3 , OH, and HO_2) were comprehensively investigated at the CCSD(T)/cc-pVXZ (X=D, T)//M06/cc-pVTZ level of theory. Rate constants were computed using TST coupled with 1D hindered rotor approximation and asymmetric Eckart tunneling effect. The H-abstractions from the α -carbon (i.e. methylene

1
2
3 group) are energetically favored due to the relatively lower energy barriers. Among H/O/CH₃ +
4
5 EF reactions, CH₃ + EF presents the lowest overall rate constant and H + EF appears with the
6
7 highest rate constants. For OH/HO₂ + EF reactions, the reactant and product H-bond complexes
8
9 were theoretically identified, but neglected reasonably in rate constant calculations due to their
10
11 minor contributions under the current high temperature conditions. The rate constants for OH +
12
13 EF → Products were measured in the shock tube using UV absorption of hydroxyl over the
14
15 temperature range of 900–1321 K and pressures of 1.4–2.0 atm. Our calculations are in excellent
16
17 agreement (within 15%) with the experimental results, which validates the accuracy of our
18
19 theoretical methods. Finally, the branching ratios derived from these site-specific rate constants
20
21 were analyzed to provide further insight into the product yields of EF pyrolysis and oxidation.
22
23
24
25
26
27
28
29
30

31 **Supporting Information**

32
33
34 The optimized geometries of reactants, products and transition states, site-specific rate
35
36 constants are provided in the Supporting Information. This information is available free of
37
38 charge via the Internet at <http://pubs.acs.org>.
39
40
41
42
43

44 **Acknowledgments**

45
46
47 The authors are very grateful to Dr. Lidong Zhang at University of Science and Technology
48
49 of China and Dr. Peng Zhang at Hong Kong Polytechnic University for the discussion on rate
50
51 constant calculations. We are also thankful for Shenzhen Supercomputing Center for providing
52
53 computational facilities. This work is supported by National Natural Science Foundation of
54
55 China (11502222) and Research Grants Council of the Hong Kong SAR, China (14234116).
56
57
58
59
60

Shock tube experiments were carried out at King Abdullah University of Science and Technology (KAUST) and this work was funded by Competitive Center Funding (CCF) program at KAUST.

References

- (1). Hill, J.; Nelson, E.; Tilman, D.; Polasky, S.; Tiffany, D. Environmental, economic, and energetic costs and benefits of biodiesel and ethanol biofuels. *Proc. Natl. Acad. Sci. U S A* **2006**, *103* (30), 11206-11210.
- (2). Ivanov, B.; Stoyanov, S. A mathematical model formulation for the design of an integrated biodiesel-petroleum diesel blends system. *Energy* **2016**, *99*, 221-236.
- (3). Prueksakorn, K.; Gheewala, S. H.; Malakul, P.; Bonnet, S. Energy analysis of Jatropha plantation systems for biodiesel production in Thailand. *Energy Sustain. Develop.* **2010**, *14* (1), 1-5.
- (4). Coniglio, L.; Bennadji, H.; Glaude, P. A.; Herbinet, O.; Billaud, F. Combustion chemical kinetics of biodiesel and related compounds (methyl and ethyl esters): experiments and modeling—advances and future refinements. *Prog. Energy Combust. Sci.* **2013**, *39* (4), 340-382.
- (5). Yusoff, M. F. M.; Xu, X.; Guo, Z. Comparison of fatty acid methyl and ethyl esters as biodiesel base stock: a review on processing and production requirements. *J. Am. Oil Chem. Soc.* **2014**, *91* (4), 525-531.
- (6). Graboski, M. S.; McCormick, R. L. Combustion of fat and vegetable oil derived fuels in diesel engines. *Prog. Energy Combust. Sci.* **1998**, *24* (2), 125-164.

- 1
2
3
4
5
6
7
8
9
10
11
12
13
14
15
16
17
18
19
20
21
22
23
24
25
26
27
28
29
30
31
32
33
34
35
36
37
38
39
40
41
42
43
44
45
46
47
48
49
50
51
52
53
54
55
56
57
58
59
60
- (7). Baiju, B.; Naik, M.; Das, L. A comparative evaluation of compression ignition engine characteristics using methyl and ethyl esters of Karanja oil. *Renew. Energy* **2009**, *34* (6), 1616-1621.
- (8). Peterson, C. L.; Reece, D. L.; Thompson, J. C.; Beck, S. M.; Chase, C. Ethyl ester of rapeseed used as a biodiesel fuel—a case study. *Biomass Bioenergy* **1996**, *10* (5-6), 331-336.
- (9). Balaganesh, M.; Dash, M. R.; Rajakumar, B. Experimental and computational investigation on the gas phase reaction of ethyl formate with Cl atoms. *J. Phys. Chem. A* **2014**, *118* (28), 5272-5278.
- (10). Kaiser, E. W. Study of the reaction Cl^+ ethyl formate at 700-950 Torr and 297 to 435 K: product distribution and the kinetics of the reaction $\text{C}_2\text{H}_5\text{OC}(\text{=O}) \rightarrow \text{CO}_2 + \text{C}_2\text{H}_5$. *J. Phys. Chem. A* **2016**, *120* (20), 3414-3423.
- (11). Belloche, A.; Garrod, R.; Müller, H.; Menten, K.; Comito, C.; Schilke, P. Increased complexity in interstellar chemistry: detection and chemical modeling of ethyl formate and n-propyl cyanide in sagittarius B2 (N). *Astron. Astrophys.* **2009**, *499* (1), 215-232.
- (12). Chou, Y. C. A Theoretical investigation of the decomposition reactions of ethyl formate in the S_0 state. *J. Chin. Chem. Soc.* **2012**, *59* (12), 1528-1535.
- (13). Chou, Y. C. A Theoretical investigation of the decomposition reactions of ethyl formate in the S_1 and T_1 states. *J. Chin. Chem. Soc.* **2013**, *60* (6), 608-617.
- (14). Makens, R. F.; Eversole, W. Kinetics of the thermal decomposition of ethyl formate. *J. Am. Chem. Soc.* **1939**, *61* (11), 3203-3206.
- (15). Blades, A. T. The kinetics of the pyrolysis of ethyl and isopropyl formates and acetates. *Can. J. Chem.* **1954**, *32* (4), 366-372.

- 1
2
3
4
5
6
7
8
9
10
11
12
13
14
15
16
17
18
19
20
21
22
23
24
25
26
27
28
29
30
31
32
33
34
35
36
37
38
39
40
41
42
43
44
45
46
47
48
49
50
51
52
53
54
55
56
57
58
59
60
- (16). Blades, A.; Sandhu, H. The arrhenius factors for some six-center unimolecular reactions. *Int. J. Chem. Kinet.* **1971**, *3* (2), 187-193.
- (17). Balaganesh, M.; Sudhakar, G.; Rajakumar, B. Thermal decomposition of ethyl formate behind the reflected shock waves in the temperature range of 909-1258K, 29th International Symposium on Shock Waves 1, Springer: **2015**; 233-238.
- (18). Hermida-Ramón, J. M.; Rodríguez-Otero, J.; Cabaleiro-Lago, E. M. Ab initio MP2 and DFT study of the thermal Syn elimination reaction in ethyl formate. *J. Phys. Chem. A* **2003**, *107* (10), 1651-1654.
- (19). Jasper, A. W.; Pelzer, K. M.; Miller, J. A.; Kamarchik, E.; Harding, L. B.; Klippenstein, S. J. Predictive a priori pressure-dependent kinetics. *Science* **2014**, *346* (6214), 1212-1215.
- (20). Westbrook, C. K.; Pitz, W. J.; Westmoreland, P. R.; Dryer, F. L.; Chaos, M.; Osswald, P.; Kohse-Höinghaus, K.; Cool, T. A.; Wang, J.; Yang, B. A detailed chemical kinetic reaction mechanism for oxidation of four small alkyl esters in laminar premixed flames. *Proc. Combust. Inst.* **2009**, *32* (1), 221-228.
- (21). Osswald, P.; Struckmeier, U.; Kasper, T.; Kohse-Höinghaus, K.; Wang, J.; Cool, T. A.; Hansen, N.; Westmoreland, P. R. Isomer-specific fuel destruction pathways in rich flames of methyl acetate and ethyl formate and consequences for the combustion chemistry of esters. *J. Phys. Chem. A* **2007**, *111* (19), 4093-4101.
- (22). Pitz, W. J.; Naik, C.; Mhaoldúin, T. N.; Westbrook, C. K.; Curran, H. J.; Orme, J. P.; Simmie, J. Modeling and experimental investigation of methylcyclohexane ignition in a rapid compression machine. *Proc. Combust. Inst.* **2007**, *31* (1), 267-275.

- 1
2
3
4 (23). Petersen, E. L.; Kalitan, D. M.; Simmons, S.; Bourque, G.; Curran, H. J.; Simmie, J. M.
5
6 Methane/propane oxidation at high pressures: experimental and detailed chemical kinetic
7
8 modeling. *Proc. Combust. Inst.* **2007**, *31* (1), 447-454.
9
- 10 (24). Akih-Kumgeh, B.; Bergthorson, J. M. Ignition of C3 oxygenated hydrocarbons and
11
12 chemical kinetic modeling of propanal oxidation. *Combust. Flame* **2011**, *158* (10), 1877-1889.
13
14
- 15 (25). Akih-Kumgeh, B.; Bergthorson, J. M. Experimental and modeling study of trends in the
16
17 high-temperature ignition of methyl and ethyl esters. *Energy Fuels* **2011**, *25* (10), 4345-4356.
18
19
- 20 (26). Tsang, W. Chemical kinetic data base for combustion chemistry. part 3: propane. *J. Phys.*
21
22 *Chem. Ref. Data* **1988**, *17* (2), 887-951.
23
- 24 (27). Wang, Q.-D.; Wang, X.-J.; Liu, Z.-W.; Kang, G.-J. Theoretical and kinetic study of the
25
26 hydrogen atom abstraction reactions of ethyl esters with hydrogen radicals. *Chem. Phys. Lett.*
27
28 **2014**, *616*, 109-114.
29
30
- 31 (28). Zhao, Y.; Truhlar, D. G. The M06 suite of density functionals for main group
32
33 thermochemistry, thermochemical kinetics, noncovalent interactions, excited states, and
34
35 transition elements: two new functionals and systematic testing of four M06-class functionals
36
37 and 12 other functionals. *Theor. Chem. Acc.* **2008**, *120* (1-3), 215-241.
38
39
- 40 (29). Frisch, M.; Trucks, G.; Schlegel, H. B.; Scuseria, G.; Robb, M.; Cheeseman, J.; Scalmani,
41
42 G.; Barone, V.; Mennucci, B.; Petersson, G., et al. Gaussian 09, Revision A. 02, Gaussian. Inc.,
43
44 Wallingford, CT **2009**.
45
46
- 47 (30). Zheng, J.; Alecu, I.; Lynch, B.; Zhao, Y.; Truhlar, D. Database of frequency scale factors
48
49 for electronic model chemistries. <http://comp.chem.umn.edu/freqscale/version2.htm> (accessed
50
51 March 15, 2017)
52
53
54
55
56
57
58
59
60

- 1
2
3
4 (31). Lee, T. J.; Taylor, P. R. A diagnostic for determining the quality of single-reference
5
6 electron correlation methods. *Int. J. Quantum Chem* **1989**, *36* (S23), 199-207.
7
8
9 (32). Taylor, P. R. Coupled-cluster methods in quantum chemistry. In *Lecture Notes in*
10
11 *Quantum Chemistry II*, Springer: 1994; 125-202.
12
13 (33). Feller, D.; Dixon, D. A. Extended benchmark studies of coupled cluster theory through
14
15 triple excitations. *J. Chem. Phys.* **2001**, *115* (8), 3484-3496.
16
17
18 (34). Canneaux, S.; Bohr, F.; Henon, E. KiSThELP: A program to predict thermodynamic
19
20 properties and rate constants from quantum chemistry results†. *J. Comput. Chem.* **2014**, *35* (1),
21
22 82-93.
23
24
25 (35). Eckart, C. The penetration of a potential barrier by electrons. *Phys. Rev.* **1930**, *35* (11),
26
27 1303.
28
29
30 (36). Badra, J.; Elwardany, A. E.; Khaled, F.; Vasu, S. S.; Farooq, A. A shock tube and laser
31
32 absorption study of ignition delay times and OH reaction rates of ketones: 2-Butanone and 3-
33
34 buten-2-one. *Combust. Flame* **2014**, *161* (3), 725-734.
35
36
37 (37). Benson, S. W.; O'Neal, H. E. Kinetic data on gas phase unimolecular reactions; DTIC
38
39 Document: **1970**.
40
41
42 (38). Kee, R. J., F. M. Rupley, and J. A. Miller. The Chemkin Thermodynamic Data Base. No.
43
44 SAND-87-8215B. Sandia National Labs., Livermore, CA (USA), 1990.
45
46
47 (39). Davidson, D. F.; Roehrig, M.; Petersen, E. L.; Di Rosa, M. D.; Hanson, R. K.
48
49 Measurements of the OH A-X (0,0) 306 nm absorption bandhead at 60 atm and 1735 K. *J. Quant.*
50
51 *Spectrosc. Radiat. Transfer* **1996**, *55* (6), 755-762.
52
53
54
55
56
57
58
59
60

- 1
2
3
4 (40). Rea, E. C.; Chang, A. Y.; Hanson, R. K. Shock-tube study of pressure broadening of the
5
6 $A^2\Sigma^+ - X^2\Pi$ (0,0) band of OH by Ar and N₂. *J. Quant. Spectrosc. Radiat. Transfer* **1987**, 37 (2),
7
8 117-127.
9
- 10 (41). Tan, T.; Yang, X.; Krauter, C. M.; Ju, Y.; Carter, E. A. Ab initio kinetics of hydrogen
11
12 abstraction from methyl acetate by hydrogen, methyl, oxygen, hydroxyl, and hydroperoxy
13
14 radicals. *J. Phys. Chem. A* **2015**, 119 (24), 6377-6390.
15
16
- 17 (42). Georgievskii, Y.; Klippenstein, S. J. Strange kinetics of the C₂H₆+ CN reaction explained.
18
19 *J. Phys. Chem. A* **2007**, 111 (19), 3802-3811.
20
21
- 22 (43). Wigner, E. On the penetration of potential energy barriers in chemical reactions. *Z Phys*
23
24 *Chem Abt B* **1932**, 19, 203-216.
25
26
- 27 (44). Marshall, P. and Glarborg, P. Ab initio and kinetic modeling studies of formic acid
28
29 oxidation. *Proc. Combust. Inst.* 2015, 35 (1), 153-160.
30
31
- 32 (45) Tan, T.; Pavone, M.; Krisiloff, D.B.; Carter, E.A. Ab initio reaction kinetics of hydrogen
33
34 abstraction from methyl formate by hydrogen, methyl, oxygen, hydroxyl, and hydroperoxy
35
36 radicals. *J. Phys. Chem. A* **2012** 116(33), 8431-8443.
37
38
- 39 (46) Dooley, S.; Burke, M.P.; Chaos, M.; Stein, Y., Dryer, F.L., Zhukov, V.P., Finch, O.,
40
41 Simmie, J.M. and Curran, H.J. Methyl formate oxidation: Speciation data, laminar burning
42
43 velocities, ignition delay times, and a validated chemical kinetic model. *Int. J. Chem. Kinet.* **2010**
44
45 42(9), 527-549.
46
47
- 48 (47) Mendes, J.; Zhou, C.W.; Curran, H.J. Theoretical and kinetic study of the hydrogen atom
49
50 abstraction reactions of esters with HO₂ radicals. *J. Phys. Chem. A* **2013** 117(51),14006-14018.
51
52
53
54
55
56
57
58
59
60

- 1
2
3
4
5
6
7
8
9
10
11
12
13
14
15
16
17
18
19
20
21
22
23
24
25
26
27
28
29
30
31
32
33
34
35
36
37
38
39
40
41
42
43
44
45
46
47
48
49
50
51
52
53
54
55
56
57
58
59
60
- (48) Tan, T., Yang, X., Ju, Y. and Carter, E.A. Ab initio kinetics studies of hydrogen atom abstraction from methyl propanoate. *Physical Chemistry Chemical Physics*, **2016** 18(6), 4594-4607.
- (49) Metcalfe, W. K.; Togbé, C.; Dagaut, P.; Curran, H. J.; Simmie, J. M. A jet-stirred reactor and kinetic modeling study of ethyl propanoate oxidation. *Combust. Flame* **2009**, 156 (1), 250-260.
- (50) Pang, G. A.; Hanson, R. K.; Golden, D. M.; Bowman, C. T. High-temperature measurements of the rate constants for reactions of OH with a series of large normal alkanes: n-Pentane, n-Heptane, and n-Nonane. *Z. Phys. Chem.* **2011**, 225 (11-12), 1157-1178.

TOC Graphic

